Nanoscale

Accepted Manuscript

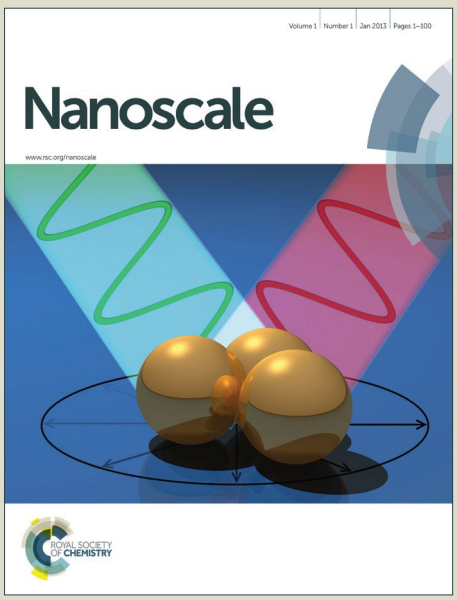

ROYAL SOCIETY OF CHEMISTRY

www.rsc.org/nanoscale

Nanoscale

COMMUNICATION

Plasmonic-Enhanced Perovskite-Graphene Hybrid Photodetectors

Zhenhua Sun,*[a, b] Lionel Aigouy[b] and Zhuoying Chen*[b]

Received 00th January 20xx,
Accepted 00th January 20xx

DOI: 10.1039/x0xx00000x

www.rsc.org/nanoscale

Surface plasmonic effect of metal nanostructure is a promising method to boost the performance of optoelectronic devices such as solar cells and photodetectors. In this report, gold nanoparticles with surface plasmon resonance localized at about 530 nm were synthesized and integrated into graphene/methylammonium lead iodide perovskite ($CH_3NH_3PbI_3$) hybrid photodetectors. Compared with pristine graphene-$CH_3NH_3PbI_3$ devices, the device with gold nanoparticles embedded has doubly higher photo-responsivity as well as faster photoresponse speed. The present devices adopt an unique configuration with gold nanoparticles physically separated from the light harvesting component, i.e., perovskite layer by graphene. Advanages are revealed through a series of characterizations and analysis. First, thanks to the tiny thickness of graphene, the plasmonic effect of gold nanoparticels can effectively enhance the near-field of perovskite and thus facilitate light-harvesting. Second, the enhanced light-harvesting in perovskite happens very closed to this interface where photo-induced carriers have relatively short paths to diffuse toward graphene, favoring fast photo-response. This work demonstrates a feasible and inspiring strategy to improve the performance of photodetectors through the surface plasmonic effect of metallic nanostructures.

Introduction

Concerning high-performance photodetectors, devices based on hybrid materials comprising graphene and light sensitive materials have attracted vast attentions. This hybrid material system can take advantage of both the high carrier mobility of graphene and the strong absorption coefficient of the light-sensitive materials thus simultaneously maximizing both light-harvesting and photo-induced carriers extraction. Upon this concept, a variety of high-performing photodetectors have been reported such as ultraviolet photodetectors based on graphene-ZnO hybrid with photo-responsivity of 22.7 A W^{-1} , infrared photodetectors based on graphene-lead sulfide quantum dots hybrid with photo-responsivity up to 10^7 A W^{-1}, and visible sensitive devices based on graphene-silicon hybrid structures.[1-6] In term of light sensitive materials, Organic-inorganic hybrid metal-halide perovskite materials (OHMPs) such as $CH_3NH_3PbI_3$ are under intense investigation for their applications in solar cells.[7-9] The power conversion efficiency of solar cells based on metal-halide perovskites is now reaching ~20%.[10, 11] This progress is mostly due to the excellent material properties including high absorption efficient, long exciton diffusion length and absence of deep traps in the band structure.[7-9, 12] Obviously these properties also make perovskites a good candidate of light sensitive materials in photodetectors. Since 2014, various photodetectors based on pure OHMPs have been reported.[13-20] Through deliberate design on either device configuration or material morphology, photodetectors with attractive features such as broad band, flexible and fast response speed were demonstrated. Nevertheless, their photo-responsivities are relative inferior, with the highest record of 340 A W^{-1}.[19] By integrating graphene into the OHMPs photodetectors forming OHMPs-graphene hybrid active layers, this value has been elevated up to 10^6 A W^{-1} in the visible range.[21-23] These works suggest the important application potential of metal-halide perovskite materials in photodetectors. Despite these promising results, further increase of the light harvesting efficiency in perovskite-based photodetectors is still necessary for devices to achieve high performance without increasing their thickness and thus favouring practical utility. To do so, the harness of plasmonic effect of nanostructure has been proven to be a feasible route.[24-29] Here we demonstrate a significant responsivity enhancement in methylammonium lead iodide perovskite ($CH_3NH_3PbI_3$)-graphene hybrid photodetectors through the insertion of gold nanoparticles (Au-NPs) into the devices. The

[a] College of Optoelectronic Engineering, Shenzhen University, Shenzhen, 518000, China.
E-mail: szh@szu.edu.cn
[b] LPEM, PSL Research University, ESPCI-ParisTech, 10 rue Vauquelin, F-75231 Paris Cedex 5, France;
CNRS, UMR8213, F-75005 Paris, France;
Sorbonne Universités, UPMC Univ Paris 06, F-75005 Paris, France.
E-mail: zhuoying.chen@espci.fr
Electronic Supplementary Information (ESI) available: See DOI: 10.1039/x0xx00000x

surface plasmonic effect of Au-NPs increases the light absorption cross-sections of the surrounding perovskite material and thus leads to higher external quantum efficiency (EQE) and responsivity.

Results and discussions

Au-NPs with a diameter of ~ 40 nm were synthesized according to a sodium citrate reduction method.[30] To integrate Au-NPs into perovskite $CH_3NH_3PbI_3$-graphene (denoted as P-G hereinafter) hybrid devices, Au-NPs were bonded on the Si/SiO_2 substrates through a self-assembled monolayer of 3-aminopropyl-triethoxysilane (APTES).[31] Fig. 1a shows a representative SEM image of Au-NPs-coated Si/SiO_2 substrate. It can be clearly seen that one layer of Au-NPs densely covers the substrate. Despite the formation of some small clusters, most particles are isolated from each other contributing a globally uniform coverage on the substrate. The optical absorption spectra of a thin film of Au-NPs coated on glass using the same bonding method used in phototransistor devices and Au-NPs in solution are shown in Fig. 1b. The localized surface plasmon resonance (LSPR) peaks from the solution sample and the thin film sample are located at same wavelength of about 530nm, confirming the uniform dispersion for the majority of Au-NPs on substrates. Fig. 1c is the atomic-force microscopy (AFM) image of the Au-NPs-coated glass. Fig. 1d is the Scanning Near-Field Optical Microscopy (SNOM) image corresponding to the sample area shown in Fig. 1c. The magnitude of the fluorescence signal probes the extent of the near-field enhancement around Au-NPs (see supplementary information).[32, 33] Despite the fact that it was not possible to resolve an individual Au-NP, from Fig. 1d one can clearly observe near-field enhancement surrounding Au-NP clusters. In some case where a large Au-NP cluster was formed, a dark spot was visible in the middle of such cluster in the fluorescence image due to the reduced amount of laser transmitted through the sample.

The phototransistor structure based on the $CH_3NH_3PbI_3$-graphene-Au-NPs hybrid system (denoted as P-G-Au hereinafter) is illustrated in Fig. 2a. On a Si/SiO_2 substrate with Au source and drain electrodes, Au-NPs were bonded through a self-assembled monolayer of APTES as described above. Graphene was then transferred onto such Au-NPs-coated substrate, followed by the deposition of the perovskite ($CH_3NH_3PbI_3$) thin film by spin-coating of a stock $CH_3NH_3PbI_3$ solution. The detailed experimental methods are in supplementary information. Fig. 1e is the Raman spectrum of graphene on a Si/SiO_2 substrate, showing its single layer characteristic.[34] The formation of $CH_3NH_3PbI_3$ crystals was verified by powder X-ray diffraction (XRD) (XRD spectrum shown in Fig. 1f).[35] The morphology of the perovskite layer is in the form of isolated islands with a maximal island height of about 400 nm (Fig. S1). With such device configuration, the interface between graphene and $CH_3NH_3PbI_3$ is intact after the integration of Au-NPs, and the $CH_3NH_3PbI_3$ layer is thin enough to be penetrated by the light used in this report.[36, 37] For comparison, the phototransistors based on graphene only and P-G were fabricated also.

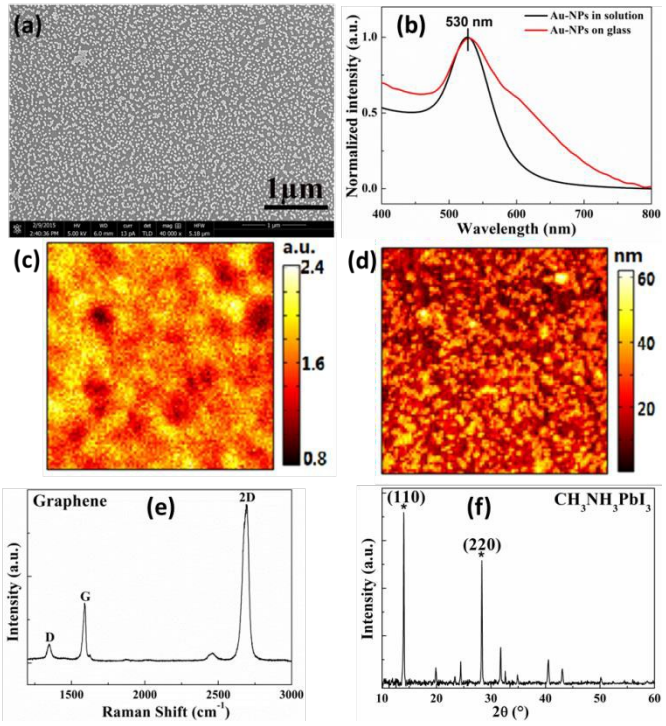

Fig. 1 (a) SEM image of Au-NPs deposited on an APTES-coated Si/SiO_2 substrate. (b) UV-Vis absorbance spectrum of Au-NPs on an APTES-coated glass. (c) AFM image of Au-NPs on an APTES-coated glass slide. The unit of the scale bar is nm. (d) The corresponding SNOM image of the same sample area as shown in (c). The brightness denotes the near-field fluorescence intensity (in arb. units). (e) Raman spectrum of graphene on Si/SiO_2 substrate upon laser excitation at 532nm. (f) XRD spectrum of the spin-coated perovskite $CH_3NH_3PbI_3$

The photo-response of graphene only, P-G and P-G-Au phototransistors were characterized systematically under the illumination of a laser (wavelength = 532 nm) operated under a series of power densities. Fig. 2b, c and d are their transfer characteristics with V_{DS} = 0.1 V under light with variable illumination intensity. Due to the non-continuous or island-like morphology, the layers of Au NPs and $CH_3NH_3PbI_3$ were determined to be nonconductive (Fig. S2). The transfer characteristics measured thus originate from the charge transport in graphene. In Fig. 2b, the graphene-only device shows undetectable response to the strongest illumination. This is due to the limited light absorption coefficient of graphene at this wavelength as well as the fast carrier recombination in pristine single layer graphene.[38, 39] Fig. 2c shows that similar graphene device with $CH_3NH_3PbI_3$ deposited above becomes strongly p-doped. This is consistent with a previous report and such p-doping can be understood by considering the electronic energy level alignment between the two materials.[22] The current in the hole wing of P-G hybrid device increases under illumination with increasing light illumination, well coincident with the negative gating effect model:[1, 22] $CH_3NH_3PbI_3$ is first excited by incident photons and thus generates holes and electrons. As the Femi level of graphene lies between the conduct band and valence band of

$CH_3NH_3PbI_3$, both photo-induced electrons and holes can be transferred from $CH_3NH_3PbI_3$ to graphene. The transfer of electrons is slower than holes, so that net electrons in $CH_3NH_3PbI_3$ will induce positive carriers in graphene through capacitive coupling and thus increase the current of transistor in the hole wing.[1, 4] Fig. 2d shows the representative transfer curve of P-G-Au devices. Despite the fact that the Au-NPs at the dielectric-graphene interface may perturb the charge transport channel to some extent, the transfer characteristics from P-G-Au devices resembles strongly those from P-G devices. Notably we observed a slightly decreased on/off ratio but a significantly larger photo-response in P-G-Au devices compare with P-G devices.

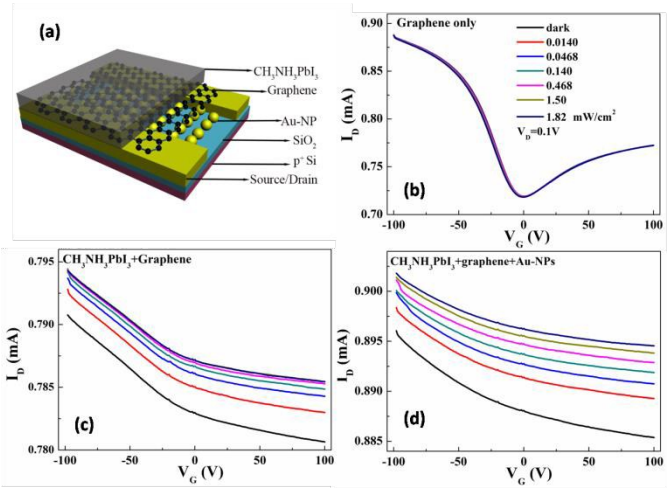

Fig. 2 (a) Schematic of the device architeture used in this study. (b), (c) and (d) Transfer characteristics of the graphene-only, $CH_3NH_3PbI_3$-graphene (P-G), and $CH_3NH_3PbI_3$-graphene-Au-NPs (P-G-Au) device, respecctively. These characteristics were measured under a V_{DS} bias of 0.1 V and under an illumination of a wavelength of 532 nm at different light intensities (listed in (b)).

To quantitatively evaluate the response improvement, the responsivities (R) and external quantum efficiencies (EQE) of P-G-Au device and P-G device at V_G of 0 V were respectively calculated through:

$$R = \frac{I_{ph}}{P} = \frac{E\mu S n_{ph}}{P} \quad (1)$$

and

$$\mathrm{EQE} = \frac{I_{ph}}{P}\frac{h\upsilon}{q} \quad (2)$$

, where, I_{ph} is the photocurrent, P the light intensity, E the applied electrical field, μ the carriers mobility, S the cross section area, n_{ph} the photo-induced carrier density, h the Planck constant, υ the light frequency, q the elemental charge.[4, 40] The calculated EQE and R were plotted along different illumination intensities and shown in Fig. 3a. Under the same illumination intensity, the P-G-Au device shows a responsivity and EQE which are almost twice higher than the P-G device. The field-effect hole mobility in P-G and P-G-Au devices were calculated to be 0.15 and 0.14 $cm^2\ V^{-1}\ s^{-1}$, respectively. From equation (1), as they have the same device structure and measured under the same condition, this responsivity increment in the P-G-Au device should originate from the increased photo-induced carriers. In principle, when the carrier injection/extraction conditions are identical, the increase of EQE represents the outcome of more carrier generation or/and less recombination. Four possible mechanisms may be responsible for the improvement according to the literature: i): The junction between Au-NPs and $CH_3NH_3PbI_3$ can facilitate the separation of excitons and the extraction of carriers; ii): the surface of Au-NPs can trap minority carriers or depress the carrier recombination in $CH_3NH_3PbI_3$; iii): hot carriers generated in Au-NPs can transfer into graphene thus increase the photocurrent; iv): the near-field enhancement in the surface of Au-NPs due to the plasmonic effect can increase the light harvesting in $CH_3NH_3PbI_3$.[26-28] In the current work, Au-NPs are not directly in contact with $CH_3NH_3PbI_3$ (there is graphene between these two materials), we therefore consider that the first and the second mechanism are unlikely the dominating process in our devices. Concerning the third mechanism, in order for the plasmonically-generated hot carrier (e.g. hot electrons) to play a role in the device performance, the Au-NPs should be in contact with a materials that can effectively remove the counter-carriers (e.g. holes). In the current work, the isolated Au-NPs are in contact with graphene and the insulating SiO_2 gate dielectric. We therefore believe that the third mechanism is also unlikely to play a significant role in the device performance observed. In reality, the transfer characteristics of a device composing only of graphene and Au-NPs show negligible response even to the strongest illumination (Fig. S3) which is similar to those observed in the graphene-only devices. We attribute the enhanced light absorption in the perovskite layer due to the plasmonic effect of Au-NPs as the main mechanism contributing to the observed increased photo-responsivity and EQE in the P-G-Au device.[29] This point will be further correlated in the following analysis.

The photo-responsivity-light intensity $R \propto P$ dependence can be fitted with power functions as shown in Fig. 3a. This relationship can be analysed using the model for carrier recombination in photovoltaic devices.[41, 42] One of the reasons for the reduced responsivity along illumination intensity is that the increased probability of carrier recombination as the carrier density increases. As illustrated in Fig. 3b, in the P-G-Au device, most photo-induced carriers are generated around the interface between graphene and perovskite (P-G interface) due to the near-field enhancement from Au-NPs. As most of these carriers are not far from the P-G interface, during their transport to graphene, the probability for them to encounter a recombination event is smaller than those carriers generated far from this interface. This contributes to the observed slower decline of responsivity along increasing light intensity in P-G-Au devices (Fig. 3a). These two devices were further characterized as photoconductors by fixing V_G to 0 V. The $R \propto V_{DS}$ dependence under variable illumination intensities are exhibited in Fig. 3c. The photo-responsivity of the P-G-Au device is twice larger than the P-G device across all illumination intensity range and under different V_{DS} (from 0 to

10 V). The responsivity values under the smallest illumination intensity (1.4×10^{-5} W cm^{-2}) and under three different V_{DS} bias (0.1, 5 and 10 V) are listed in Table 1. The maximum photo-responsivity value observed reaches up to 2×10^3 A W^{-1} with V_{DS} = 10 V. The responsivity value is not extraordinarily high, but the point in this report is a reliable enhancement effect instead of a record value. The performances of some photodetectors based on graphene and OHMPs hybrids in literatures are listed in Table 2 for comparison. Note that, first, the responsivity value will be larger under weaker light illumination. Second, such responsivity value depends on the carrier mobility of graphene. Higher responsivity can be expected if graphene of improved quality (e.g. in terms of defects, grain boundaries, and uniformity) is applied. The $R \propto P$ dependences at different V_{DS} was extracted and plotted in Fig. 3d. These curves can be fitted well by power functions and the fitting results are shown in Fig. 3d. The $R \propto P$ relationships are near identical comparing Fig. 3a and d, suggesting the plasmonic enhanced responsivity is not dependent on the lateral source-drain field.

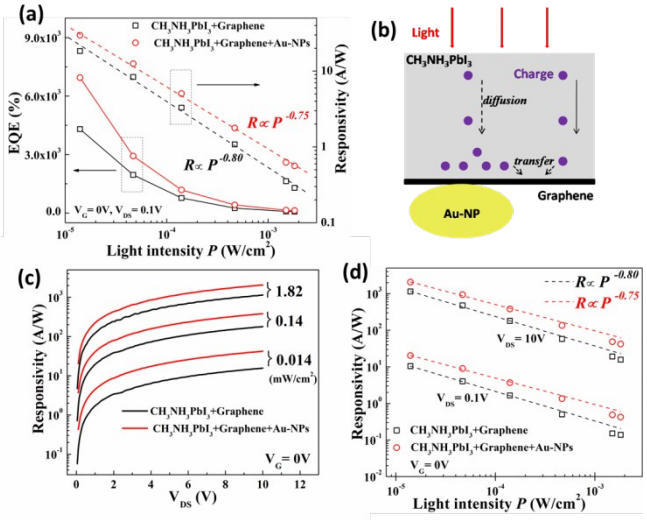

Fig. 3 (a) The photo-responsivities and external quantum efficiency (EQE) vs. light intensity relationships for the G-P and G-P-Au devices. Data were extracted from the transfer characteristics of the respective device at zero gate voltage as shown in Figure 2(c) and (d). The dependences of responsivities on light intensity are fitted with power functions with fitting parameters listed in (a). (b) Schematic of generation, diffusion and transfer of photo-induced carriers in the perovskite layer with and without the influence of gold nanoparticles. (c) Responsivities vs VDS under different light intensities. d) Responsivities vs. light intensity at different VDS bias. The dependences of responsivities on light intensity are fitted with power functions with fitting parameters listed in (d).

Table 1 Photo-responsivities (R) of P-G and P-G-Au devices under same laser illumination (wavelength = 532 nm, intensity = 1.4×10^{-5} W cm^{-2}) and different V_{DS} bias (0.1, 5 and 10 V).

V_{DS}	0.1 V	1 V	10 V
R (P-G)	10.4 A W^{-1}	122.0 A W^{-1}	1142.9 A W^{-1}
R (P-G-Au)	20.4 A W^{-1}	223.5 A W^{-1}	2067.1 A W^{-1}

The photo-switching characteristics of these two photodetectors were determined under a periodic on-off illumination (wavelength = 532 nm, intensity = 1.82 mW cm^{-2}) and a V_{DS} of 0.1 V without gate bias (Fig. 4a). Both of the P-G-Au and P-G devices exhibit stable performance with cyclic photocurrents following light signals. The photocurrent of P-G-Au device is significantly higher than the P-G device, coherent with the steady device characteristics mentioned above. A representative one cycle response is shown in Fig. 4b. The response time is defined as the time used for photocurrent to increase from null to the 80% of the saturation level.[1] It can be observed that the P-G-Au device responses slightly faster than the P-G device. This can be well explained by the model illustrated in Fig. 3b. In the P-G-Au device, the existence of Au-NPs leads to more photo-induced carriers generated in the perovskite layer near the P-G interface. The time for these carriers to diffuse to graphene is shorter than carriers generated far from the P-G interface, thus lead to the observed faster operation in the P-G-Au device compared with the P-G device. It is worth noting that slow response speed is an inherent pitfall in graphene-light absorber hybrid photodetectors.[4] In these devices, photo-induced carriers have to travel across a long distance before injected into graphene and then extracted out from electrodes. Enhancing carriers generation in light absorber near graphene by surface plasmonic effect of metal nanoparticles is thus a feasible way to accelerate the photo-response speed in this type of photodetectors. The stability of photodetectors is an important figure of merit toward practical applications. Most components of the device presented here are stable for months except for $CH_3NH_3PbI_3$, which will decompose in several hours under high humidity ambient conditions.[43] The search for solutions to promote the stability of devices based on $CH_3NH_3PbI_3$ as well as similar OHMP compounds is a challenging and currently ongoing topic.[44, 45] Device encapsulation may partially alleviate the stability problem.

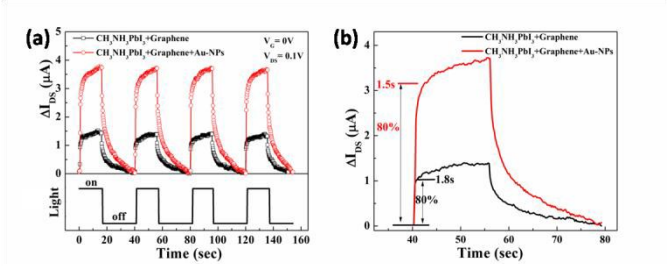

Fig. 4 (a) The photo-switching characteristics of the P-G and P-G-Au devices under alternating dark and illumination conditions (wavelength = 532 nm, intensity = 1.82 mW cm^{-2}). Dark time: 17s; light time: 23s. (b) Response time study on a single representative light/dark cycle.

Conclusions

In conclusion, the responsivities of perovskite ($CH_3NH_3PbI_3$)-graphene hybrid photodetectors under a visible illumination of a wavelength of 532 nm were enhanced doubly by integrating gold nanoparticles with a diameter of ~ 40 nm underneath the graphene. This enhancement can be attributed to the improved light harvesting in the perovskite layer due to the surface plasmonic effect of gold nanoparticles. In addition, as

Table 2 The performances of photodetectors based on graphene-OHMPs hybrids in literatures and this work. (MPbI3: $CH_3NH_3PbI_3$; $MPbBr_2I$: $CH_3NH_3PbBr_2I$; G: graphene)

Active Material	Operation wavelength (nm)	Incident Power (μW)	Responsivity (A/W)	Response Time (s)	Reference
$MPbI_3$ film + G	520	1	180	0.087 (fitting data)	Ref. 22
$MPbI_3$ nanowire + G	633	3×10^{-6}	2.6×10^6	55 (rise up to 70%)	Ref. 23
$MPbBr_2I$ island + G	405	0.001	6×10^5	0.12 (rise up to 70%)	Ref. 21
$MPbI_3$ island + G	532	0.01	1.1×10^3	1.8 (rise up to 80%)	This work
$MPbI_3$ island + G + Au-NPs	532	0.01	2.1×10^3	1.5 (rise up to 80%)	This work

the improved light harvesting in the perovskite layer mainly happens in regions close to the perovskite-graphene interface, the carriers extraction efficiency and photodetector operation speed are improved compared with devices without gold nanoparticles. This work demonstrates a functional example as well as a promising strategy to improve the performance of graphene-based photodetectors in multiple aspects simultaneously.

Acknowledgements

Z.H.S. acknowledges support from the National Natural Science Foundation of China (grant no. 61505108), the Science and Technology Innovation Commission of Shenzhen (grant no. JCYJ20150625103602228) and the Natural Science foundation of Shenzhen University (grant no. 201509). Z.H.S. and Z.C. acknowledge support from the ANR-2011-JS09-004-01-PvCoNano project and the EU Marie Curie Career Integration Grant (project no. 303824). Authors are grateful to Botao Ji for his assistance in gold nanoparticles synthesis, and Zhesheng Chen for his assistance in Raman spectrum measurement.

Notes and references

1. Z. H. Sun, Z. K. Liu, J. H. Li, G. A. Tai, S. P. Lau and F. Yan, *Adv Mater*, 2012, **24**, 5878-5883.
2. G. Konstantatos, M. Badioli, L. Gaudreau, J. Osmond, M. Bernechea, F. P. G. de Arquer, F. Gatti and F. H. L. Koppens, *Nat Nanotechnol*, 2012, **7**, 363-368.
3. H. X. Chang, Z. H. Sun, K. Y. F. Ho, X. M. Tao, F. Yan, W. M. Kwok and Z. J. Zheng, *Nanoscale*, 2011, **3**, 258-264.
4. Z. H. Sun and H. X. Chang, *Acs Nano*, 2014, **8**, 4133-4156.
5. X. M. Li, H. W. Zhu, K. L. Wang, A. Y. Cao, J. Q. Wei, C. Y. Li, Y. Jia, Z. Li, X. Li and D. H. Wu, *Adv Mater*, 2010, **22**, 2743-+.
6. X. H. An, F. Z. Liu, Y. J. Jung and S. Kar, *Nano Lett*, 2013, **13**, 909-916.
7. G. Hodes, *Science*, 2013, **342**, 317-318.
8. M. A. Green, A. Ho-Baillie and H. J. Snaith, *Nat Photonics*, 2014, **8**, 506-514.
9. M. Gratzel, *Nat Mater*, 2014, **13**, 838-842.
10. H. P. Zhou, Q. Chen, G. Li, S. Luo, T. B. Song, H. S. Duan, Z. R. Hong, J. B. You, Y. S. Liu and Y. Yang, *Science*, 2014, **345**, 542-546.
11. N. J. Jeon, J. H. Noh, W. S. Yang, Y. C. Kim, S. Ryu, J. Seo and S. I. Seok, *Nature*, 2015, **517**, 476-480.
12. G. C. Xing, N. Mathews, S. Y. Sun, S. S. Lim, Y. M. Lam, M. Gratzel, S. Mhaisalkar and T. C. Sum, *Science*, 2013, **342**, 344-347.
13. X. Hu, X. D. Zhang, L. Liang, J. Bao, S. Li, W. L. Yang and Y. Xie, *Adv Funct Mater*, 2014, **24**, 7373-7380.
14. S. F. Zhuo, J. F. Zhang, Y. M. Shi, Y. Huang and B. Zhang, *Angew Chem Int Edit*, 2015, **54**, 5693-5696.
15. K. Chen and H. Tüysüz, *Angewandte Chemie International Edition*, 2015, **54**, 13806-13810.
16. L. T. Dou, Y. Yang, J. B. You, Z. R. Hong, W. H. Chang, G. Li and Y. Yang, *Nat Commun*, 2014, **5**.
17. C. Liu, K. Wang, C. Yi, X. J. Shi, P. C. Du, A. W. Smith, A. Karim and X. Gong, *J Mater Chem C*, 2015, **3**, 6600-6606.
18. B. R. Sutherland, A. K. Johnston, A. H. Ip, J. X. Xu, V. Adinolfi, P. Kanjanaboos and E. H. Sargent, *Acs Photonics*, 2015, **2**, 1117-1123.
19. F. Li, C. Ma, H. Wang, W. J. Hu, W. L. Yu, A. D. Sheikh and T. Wu, *Nat Commun*, 2015, **6**.
20. H. Deng, X. Yang, D. Dong, B. Li, D. Yang, S. Yuan, K. Qiao, Y.-B. Cheng, J. Tang and H. Song, *Nano Lett*, 2015, DOI: 10.1021/acs.nanolett.5b03061.
21. Y. S. Wang, Y. P. Zhang, Y. Lu, W. D. Xu, H. R. Mu, C. Y. Chen, H. Qiao, J. C. Song, S. J. Li, B. Q. Sun, Y. B. Cheng and Q. L. Bao, *Adv Opt Mater*, 2015, **3**, 1389-1396.
22. Y. Lee, J. Kwon, E. Hwang, C. H. Ra, W. J. Yoo, J. H. Ahn, J. H. Park and J. H. Cho, *Adv Mater*, 2015, **27**, 41-46.
23. M. Spina, M. Lehmann, B. Nafradi, L. Bernard, E. Bonvin, R. Gaal, A. Magrez, L. Forro and E. Horvath, *Small*, 2015, **11**, 4824-4828.
24. B. A. Nie, J. G. Hu, L. B. Luo, C. Xie, L. H. Zeng, P. Lv, F. Z. Li, J. S. Jie, M. Feng, C. Y. Wu, Y. Q. Yu and S. H. Yu, *Small*, 2013, **9**, 2872-2879.
25. L. B. Luo, L. H. Zeng, C. Xie, Y. Q. Yu, F. X. Liang, C. Y. Wu, L. Wang and J. G. Hu, *Sci Rep-Uk*, 2014, **4**.
26. D. B. Li, X. J. Sun, H. Song, Z. M. Li, Y. R. Chen, H. Jiang and G. Q. Miao, *Adv Mater*, 2012, **24**, 845-+.
27. W. Zhang, J. Xu, W. Ye, Y. Li, Z. Q. Qi, J. N. Dai, Z. H. Wu, C. Q. Chen, J. Yin, J. Li, H. Jiang and Y. Y. Fang, *Appl Phys Lett*, 2015, **106**.
28. L. B. Luo, W. J. Xie, Y. F. Zou, Y. Q. Yu, F. X. Liang, Z. J. Huang and K. Y. Zhou, *Opt Express*, 2015, **23**, 12979-12988.
29. W. Zhang, M. Saliba, S. D. Stranks, Y. Sun, X. Shi, U. Wiesner and H. J. Snaith, *Nano Lett*, 2013, **13**, 4505-4510.
30. B. V. Enustun and J. Turkevich, *J Am Chem Soc*, 1963, **85**, 3317.
31. A. P. Kulkarni, K. M. Noone, K. Munechika, S. R. Guyer and D. S. Ginger, *Nano Lett*, 2010, **10**, 1501-1505.
32. L. Aigouy, P. Prieto, A. Vitrey, J. Anguita, A. Cebollada, M. U. Gonzalez, A. Garcia-Martin, J. Labeguerie-Egea and M. Mortier, *J Appl Phys*, 2011, **110**.
33. A. Vitrey, L. Aigouy, P. Prieto, J. M. Garcia-Martin and M. U. Gonzalez, *Nano Lett*, 2014, **14**, 2079-2085.
34. A. C. Ferrari, J. C. Meyer, V. Scardaci, C. Casiraghi, M. Lazzeri, F. Mauri, S. Piscanec, D. Jiang, K. S. Novoselov, S. Roth and A. K. Geim, *Phys Rev Lett*, 2006, **97**.
35. J. H. Heo, S. H. Im, J. H. Noh, T. N. Mandal, C. S. Lim, J. A. Chang, Y. H. Lee, H. J. Kim, A. Sarkar, M. K. Nazeeruddin, M. Gratzel and S. I. Seok, *Nat Photonics*, 2013, **7**, 487-492.

36. P. Loper, M. Stuckelberger, B. Niesen, J. Werner, M. Filipic, S. J. Moon, J. H. Yum, M. Topic, S. De Wolf and C. Ballif, *J Phys Chem Lett*, 2015, **6**, 66-71.
37. C. D. Bailie and M. D. McGehee, *Mrs Bull*, 2015, **40**, 681-685.
38. T. Mueller, F. N. A. Xia and P. Avouris, *Nat Photonics*, 2010, **4**, 297-301.
39. J. H. Li, L. Y. Niu, Z. J. Zheng and F. Yan, *Adv Mater*, 2014, **26**, 5239-5273.
40. G. Konstantatos and E. H. Sargent, *Nat Nanotechnol*, 2010, **5**, 391-400.
41. A. K. Rath, M. Bernechea, L. Martinez, F. P. G. de Arquer, J. Osmond and G. Konstantatos, *Nat Photonics*, 2012, **6**, 529-534.
42. Z. H. Sun, G. Sitbon, T. Pons, A. A. Bakulin and Z. Y. Chen, *Sci Rep-Uk*, 2015, **5**.
43. J. L. Yang, B. D. Siempelkamp, D. Y. Liu and T. L. Kelly, *Acs Nano*, 2015, **9**, 1955-1963.
44. G. D. Niu, X. D. Guo and L. D. Wang, *J Mater Chem A*, 2015, **3**, 8970-8980.
45. J. You, L. Meng, T.-B. Song, T.-F. Guo, Y. Yang, W.-H. Chang, Z. Hong, H. Chen, H. Zhou, Q. Chen, Y. Liu, N. De Marco and Y. Yang, *Nat Nano*, 2016, **11**, 75-81.